MONITORING THE MOISTURE INGRESS INTO PV MODULES BY MEASURING CAPACITIVE CHARACTERISTICS

Esther Fokuhl, Heinrich Berg, Sandor Stecklum, Djamel Eddine Mansour, Daniel Philipp, Paul Gebhardt
Fraunhofer Institute for Solar Energy Systems
Heidenhofstr. 2, 79110 Freiburg, Germany

ABSTRACT: We are presenting an approach for the monitoring of the parasitic capacitance of PV modules as an indication for moisture ingress into the polymers during artificial aging tests. The setup can be used on commercially available modules and prototypes without complex sample preparation. Influences on the measurement result like temperature and humidity dependence are investigated. First measurements during damp heat show promising results for framed full-size and mini-modules.
Keywords: Experimental Methods, Impedance, Monitoring

1 INTRODUCTION

Humidity is one of the main stress factors during the lifetime of PV modules. Moisture diffusion into PV modules can lead to mechanical stress due to the hygroscopic expansion of polymeric layers or enhance thermomechanical stress at temperature changes [1]. Furthermore, water can cause hydrolysis of polymers or the corrosion of metallic components and can be a reactant in chemical reactions resulting in acetic acid formation [2]. Humidity also plays an important role in case of PID as the conductivity of the module surface and the polymeric layers is crucial for the leakage current density and therefore has a significant influence on the degradation speed [3].

Monitoring the moisture ingress into PV modules can be desirable to understand degradation mechanisms during accelerated or natural aging and for the development of accelerated testing methods. Other possible applications are the comparison of material combinations and module designs, the correlation of new test conditions with standard tests (e.g. pressure cooker test vs. damp heat) and the validation of FEM models.

Jankovec et al. have proposed a moisture monitoring method based on module integrated digital temperature and relative humidity sensors [4]. Their monitoring setup has later been used to compare and verify simulation models for moisture diffusion [5].

In this work, we are monitoring changes in the parasitic capacitance of PV modules as an indication for moisture ingress. The general feasibility of the approach has already been shown in [6] for standard modules and various measurement devices. We are following up with this work by performing a capacitance monitoring on standard modules and 4-cell modules, comparing three different electrode designs. As an advantage over module integrated sensors, our setup can be used on commercially available modules and prototypes without complex sample preparation.

2 APPROACH

2.1 Theoretical background

Due to their geometry, PV modules contain an undesired parasitic capacitance between frame or mounting system and the cells. During operation, this capacitance can cause displacement currents, also known as capacitive leakage currents, which may lead to inverter shutdowns. We are benefiting from the capacitive characteristics of PV modules by using changes in impedance values as an indication for moisture ingress.

In the exemplary structure of a 4-cell mini-module illustrated in Figure 1, the insulating materials glass, encapsulant and back sheet function as dielectrics of a capacitor.

The capacitance C of a capacitor of any desired geometry can be described by

$$C = \frac{Q}{U} = \varepsilon_0 \varepsilon_r \frac{\oint\!\!\oint_A \vec{E} \cdot d\vec{A}}{\int_s \vec{E} \cdot d\vec{s}} \qquad (1)$$

with Q = electric charge, U = applied voltage, ε_0 = dielectric constant, ε_r = relative permittivity, E = electric field strength, A = area, s = distance.
As can be derived from equation (1), C is linearly dependent on the relative permittivity ε_r.
Characteristic values for ε_r of module materials and water are given in Table I. Within this work, we are using measurement frequencies between 100 Hz and 100 kHz. At these frequencies, we can assume ε_r of water to be close to the static values and therefore close to 59 at 85 °C. With increasing moisture concentration in the polymer layers we expect an increase of the permittivity leading to an increase of the capacitance.

Figure 1: Simplified cross-section through a 4-cell mini module (not scaled). Shown components: frame (black), front glass (grey), encapsulant (peach), cells (blue), back sheet (green)

Table I: Relative permittivity values for PV module materials. *interpolated from [7]; **interpolated from [8]

Material	$\varepsilon_{r,\,static}$ at 25 °C	$\varepsilon_{r,\,static}$ at 85 °C	$\varepsilon_{r,\,\infty}$ at 25 °C	$\varepsilon_{r,\,\infty}$ at 85 °C
Glass	5…10 [9]			
Polymers	< 4 [10]	< 4 [10]	< 4 [10]	< 4 [10]
Water	80.27 [7]	≈ 59*	3.25 [8]	≈ 2.64**

2.1 Measurement setup

We have realized an automated measurement setup as shown in Figure 2. The measurement device, an LCR meter of type Agilent 4327B, is determining real and imaginary components of impedance values by measuring the voltage over and current through a test device. The test voltage used within this work is 1 V_{rms},

which is the highest possible voltage offered by the LCR meter. We used all available frequencies, namely 100 Hz, 120 Hz, 1 kHz, 10 kHz and 100 kHz in order to evaluate suitable frequencies and achieve information on frequency dependencies.

The LCR meter is connected to a datalogger (Agilent 34970 A) with up to three measurement cards used as switch units. This way, numerous test samples can be monitored simultaneously.

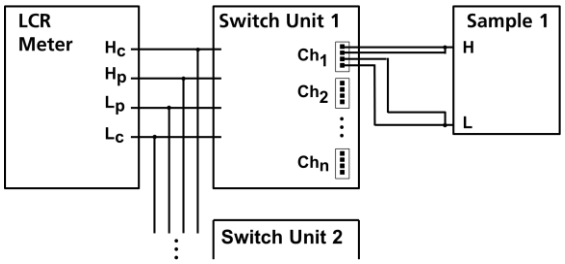

Figure 2: Schematic diagram of the measurement setup. Hc – High current; Hp – High potential; Lp – Low potential; Lc – Low current; Ch – Channel

2.3 Sample preparation

We have prepared various 4-cell-modules and two standard 60-cell modules for capacitive moisture monitoring during a damp heat test (85 °C and high relative humidity, e.g. 85 %). For the capacitance measurements, the electrode designs exemplarily shown in Figure 3 are used. In all designs, the positive electrode is formed by the short circuited cells of the module. The negative electrode is built by either

a) the module frame (see Figure 1)
b) a full size front electrode, realized by adhesive copper foil
c) a "pseudo frame", realized by stripes (width = 1 cm) of adhesive copper foil along three edges of the front glass

The motivation behind variations in electrode design is on the one hand to be able to apply the measurement on various module constructions, independent of the presence of a frame. On the other hand, different electrode designs might be sensitive to moisture ingress in different regions of the module, e.g. between cell and frame (designs a and c) or between cell and front glass (design b). A change in electrode geometry might therefore allow monitoring the moisture in specific locations or materials of the module.

In design a, the negative electrode has been attached to the frame by using a ring cable lug crimped on the cable, combined with a stainless steel nut, bolt, and star washer. In designs b and c, the electrical connection has been realized by soldering.

(a) (b) (c)

Figure 3: Exemplary 4-cell modules that have been prepared for the moisture monitoring: framed module (a), framed module with front electrode (b) and frameless module with simulated frame (c)

3 INFLUENCES ON THE MEASUREMENT

Before applying damp heat conditions, we investigate influences on the measurement results which are not related to moisture diffusion.

3.1 Capacitance of the measurement setup

As the LCR meter is not directly connected to the tested samples (see Figure 2), the electrical properties of cables and switching units contribute to the measured impedance values. Measurements on this part of the measurement setup showed mainly capacitive behavior with a phase shift between current and voltage of $\varphi \approx -90°$. We therefore consider the measurement setup simplified as a capacitor C_{MS} parallel to the sample. Using this assumption, we can determine the capacitance of the sample by subtracting C_{MS} from the measured capacitance values C_{measured}.

Temperature dependent values for C_{MS} measured on four exemplary cables with a cable length of 1.5 m while using three measurement cards as switching units, are given in Figure 4. During the measurement, the LCR meter and the switching units were placed next to the climate chamber, while the cables were passed through a cable bushing into the climate chamber, similar to during operation with test samples.

The measured capacitance values show weak negative temperature dependence. At 85 °C, C_{MS} for the exemplary cables was approximately 288 pF ± 2 pF.

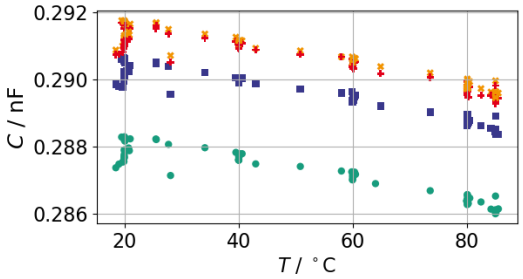

Figure 4: Temperature dependent capacitance values measured with f = 1 kHz on four cables connected to the measurement setup (3 measurement cards, cable length: 1.5 m). Different colors and styles depict different cables.

3.2 Temperature dependence of the test samples

In order to investigate the temperature dependence of the capacitance of the samples described in 2.3, we have performed a temperature test. The temperature in the climate chamber was set to five temperature steps between 20 °C and 85 °C by ramping while the humidity was not controlled. After a set point was reached, steady state was kept for at least 1 h.

Figures 5 and 6 show the corrected capacitance values (after subtracting C_{MS}) of two identically constructed 60-cell modules with polymeric back sheet and the electrode designs a (frame) and b (full front electrode) in dependence of the climate chamber temperature at various frequencies.

For both electrode designs, the capacitance values show nonlinear temperature dependence with a stronger increase at low frequencies. At 100 Hz, the capacitance changes about 13.6 % (design a) and 35.5 % (design b) between 20 °C and 85 °C. At 1 kHz and 100 kHz, changes of 4.1 % and 0.6 % (design a), respectively 13.0 % and 1.6 % (design b) have been observed.

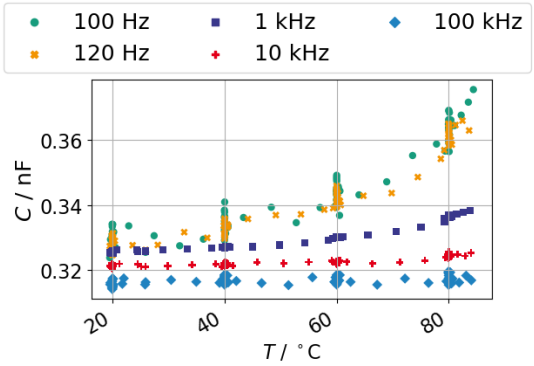

Figure 5: Temperature dependent capacitance values between short-circuited cells and frame of a 60-cell module at various frequencies (design a).

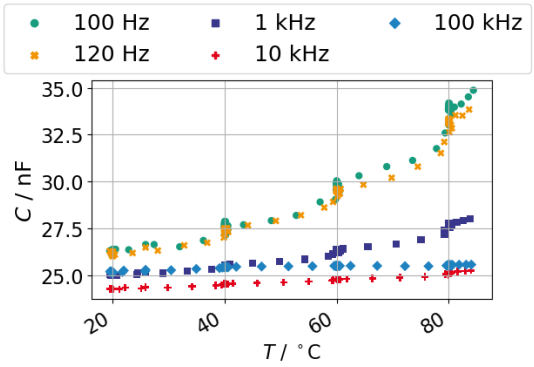

Figure 6: Temperature dependent capacitance values between short-circuited cells and full-size front electrode of a 60-cell module at various frequencies (design b).

3.3 Humidity dependence of the test samples

Figures 7 and 8 show the measured capacitance values of the 60-cell modules with electrode designs a and b in dependence of the relative humidity *RH* in the climate chamber during the ramp-up phase before damp heat at 85 °C. Within the timeframe of the experiment, only a negligible amount of moisture ingress into the module was assumed For electrode design a (Figure 7), strong humidity dependence can be seen for frequencies ≤ 1 kHz at $RH \geq 60$ %. At 100 Hz, the increase of *RH* from 60 % to 85 % leads to a capacitance increase of ≈ 64 %. At 1 kHz and 100 kHz, overall capacitance changes of ≈ 15 % and ≈ 1 % have been derived. The strong increase in capacitance at low frequencies can be explained with the increase in surface conductivity due to adsorption.

For electrode design b (Figure 8), the values are almost constant and no clear humidity dependence is observed. As the module has a full side front electrode, adsorption at the front side does not contribute to a higher surface conductivity and therefore not increase the capacitance value.

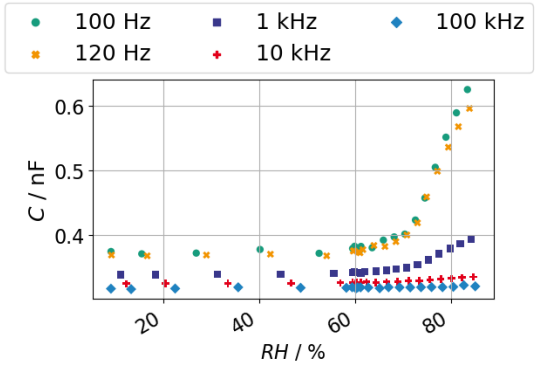

Figure 7: Humidity dependent capacitance values between short-circuited cells and frame of a 60-cell module at various frequencies and 85 °C (design a).

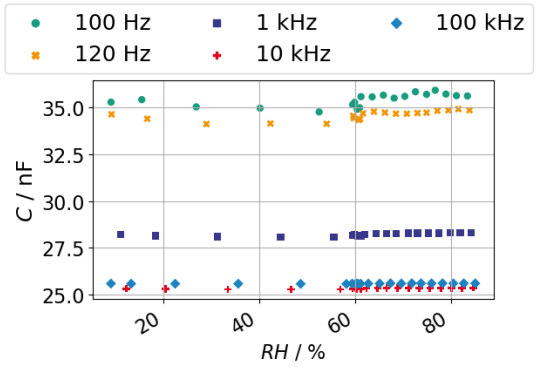

Figure 8: Humidity dependent capacitance values between short-circuited cells and full-size front electrode of a 60-cell module at various frequencies and 85 °C (design b).

3.4 Conclusions for the application of moisture monitoring

The measured capacitance values contain the capacitance of the measurement setup with not negligible values in the range of up to 300 pF, depending on the cable length and the number of switch units. As the measurement devices are kept at room temperature and the cable capacitance features only low temperature dependence we expect this influence to be a constant value during damp heat, which can be determined prior to an experiment.

The strong sensitivity of the measured capacitance values towards changes of the sample temperature and relative humidity is a possible error source especially at low frequencies if the control and distribution of *T* and *RH* in the climate chamber is not constant.

4 CAPACITANCE MONITORING DURING DH

4.1 Test conditions

A damp heat test has been performed on the two 60-cell modules with polymeric back sheet and electrode designs a and b and numerous 4-cell-modules with different material combinations and electrode designs a, b and c. In this work, we are focusing on res

ults achieved for the two 60-cell modules and two identically constructed 4-cell modules with EVA as encapsulant and PET back sheet.

During the test, the samples were placed vertically in a climate chamber. To ensure electrical insulation, silicone stripes and / or pieces of Teflon were placed under the samples.
The test conditions were:

$0 \leq t \leq 100$ h:
- T = 85 °C ± 0.5 °C
- RH = 78 % ± 3 %

t > 100 h:
- T = 85 °C ± 0.5 °C
- RH = 85 % ± 3 %

4.2 Results

The progress of capacitance change ΔC measured for a 60-cell module with electrode design a during 200 h damp heat is shown in Figure 9. At frequencies ≤ 10 kHz, a continuous increase of the capacitance can be observed during the first 100 h, while the conditions were 85 °C and 78 % *RH*. After the humidity is increased to 85 % at t = 100 h, an abrupt capacitance shift is followed by an increase of the slope. The high frequency dependence of the slope is remarkable. After 190 h, the capacitance change at a frequency of 100 Hz is approximately 440 pF or 69 %. As a comparison, at 1 kHz, a capacitance change of 90 pF or 23 % is observed. This effect is in accordance with [11,12], who explained frequency dependent changes of capacitive humidity sensors by polarization effects of water molecules, which are strongest at low frequencies.

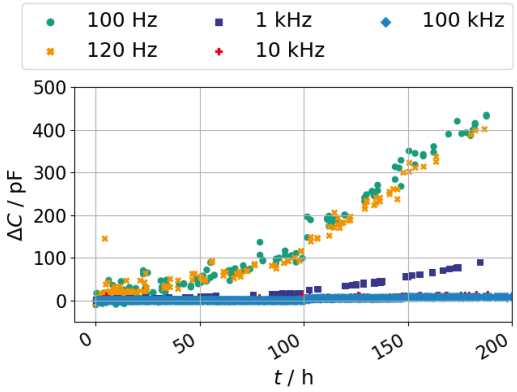

Figure 9: Capacitance change between short-circuited cells and frame of a 60-cell module during damp heat at various frequencies (design a).

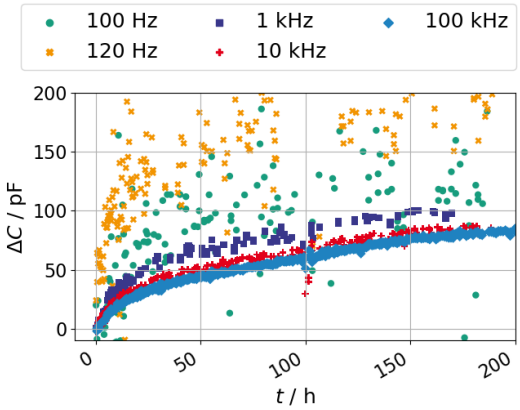

Figure 10: Capacitance change between short-circuited cells and full-size front electrode of a 60-cell module during damp heat at various frequencies (design b).

The capacitance changes of the 60-cell module with electrode design b show a different progression. At all frequencies, the slope is highest during the first hours of monitoring. After 50 h, more than half of the change observed after 200 h is completed. The measurement values show only low frequency dependence. At f ≥ 1 kHz, the overall measured change is in the range of 80 pF to 100 pF. After increasing the relative humidity to 85 %, no shift or change in slope is detected. We therefore assume that the changes seen with electrode design b within the first 200 h do not correlate to moisture ingress but are caused by other effects that are yet to be explained. As the capacitance of the sample is high, the relative changes due to these unknown effects are comparably low (0.28 % to 0.3 %). As the electric field with electrode design b is strongest between cell and front electrode, changes correlating with moisture diffusion might be seen after a longer testing time, when the moisture increase in front of the cells is higher.

To evaluate the applicability for smaller samples and to compare electrode designs a and c, we are showing the results of two identically constructed 4-cell modules with EVA as encapsulant and PET back sheet at a measurement frequency of 1 kHz (see Figure 11). Due to sample size and probe geometries, the capacitance values measured at 1 kHz at the beginning of the test were 75 pF for the framed 4-cell module (design a) and 34 pF for the module with pseudo-frame (design c). These values are significantly lower than the capacitance measured for the 60-cell module with electrode design a (≈ 620 pF at t = 0 and f = 1 kHz). The shape of the curves is qualitatively comparable to the progress of capacitance change of the 60-cell module with electrode design a at 1 kHz (see Figure 9) though they only show a minor increase in slope when the relative humidity is increased to 85 % after 100 h. The changes in capacitance during 200 h amount to 15 pF and 20 pF or 44 % (design c) and 27 % (design a). In case of the module with electrode design c, some values at t > 100 h indicates an influence of disturbance variables on the measurement result, which might be more significant when the capacitance of the sample is comparably low.

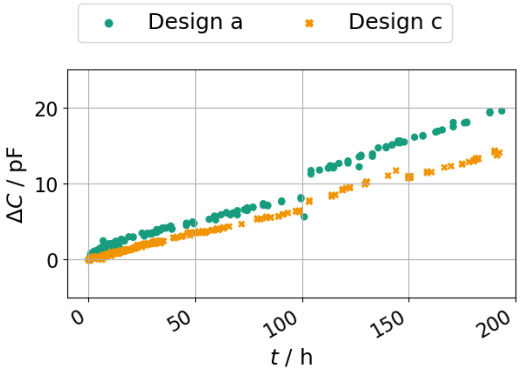

Figure 11: Change of capacitance during damp heat at 1 kHz. Samples: two 4-cell modules with frame (design a) and pseudo frame (design c).

5 CONCLUSIONS AND OUTLOOK

The presented measurement approach seems to be suitable to monitor moisture ingress into PV modules under constant climatic conditions. The results of a 60-cell module with polymeric back sheet which was connected between short-circuited cells and frame show

an increase in capacitance that corresponds well with the expected moisture increase in the polymers of the module. In case of electrode design b (front electrode), we could not identify capacitance changes which are correlated to moisture ingress within 200 h. One possible reason is that longer testing time is necessary to reach a significant increase in moisture concentration between cell and front glass, where the strongest influence on the capacitive values is expected for this electrode design. Results on 4-cell modules show, that the method is also applicable for prototype samples with a smaller form factor. For frameless modules, a pseudo-frame made of adhesive cupper foil can be an alternative. However, if the capacitance values of the tested sample are low, the measurement might be more sensitive to disturbing influences. Especially the capacitance changes of the module with design b indicate that influences, which are not fully understood yet, might be relevant for the measurement results.

To validate and quantify the measurement, a comparison with other measurement methods and simulation results will be done in the future.

6 ACKNOWLEDGEMENTS

This work has been funded by the German Federal Ministry for Economic Affairs and Energy (BMWi) in scope of the project “HJT 4.0” (contract number 0324172B).

7 REFERENCES

[1] Rashtchi S, Ruiz PD, Wildman R, Ashcroft I. Measurement of moisture content in photovoltaic panel encapsulants using spectroscopic optical coherence tomography: a feasibility study. In: Dhere NG, Wohlgemuth JH, editors. *Reliability of Photovoltaic Cells, Modules, Components, and Systems V:* SPIE; 2012, 84720O.

[2] Kempe MD, Jorgensen GJ, Terwilliger KM, McMahon TJ, Kennedy CE, Borek TT. Acetic acid production and glass transition concerns with ethylene-vinyl acetate used in photovoltaic devices. *Solar Energy Materials and Solar Cells* 2007;91:315–29, doi:10.1016/j.solmat.2006.10.009.

[3] Jankovec M, Galliano F, Annigoni E, Li HY, Sculati-Meillaud F, Perret-Aebi L-E, Ballif C, Topic M. <italic>In-Situ</italic> Monitoring of Moisture Ingress in PV Modules Using Digital Humidity Sensors. *IEEE J. Photovoltaics* 2016;6:1152–9, doi:10.1109/JPHOTOV.2016.2583779.

[4] Mitterhofer S, Barretta C, Castillon LF, Oreski G, Topic M, Jankovec M. A Dual-Transport Model of Moisture Diffusion in PV Encapsulants for Finite-Element Simulations. *IEEE J. Photovoltaics* 2020;10:94–102, doi:10.1109/JPHOTOV.2019.2955182.

[5] Berg H, Saw MH, Philipp D. Die parasitäre Kapazität eines PV-Moduls als Ursache für einen erhöhten Ableitstrom und Indikator für den Feuchteeintrag im Verkapselungsmaterial. *Regensburg: OTTI, 2016 (Wissen für Profis)*.

[6] Uematsu M, Frank EU. Static Dielectric Constant of Water and Steam. *Journal of Physical and Chemical Reference Data* 1980;9:1291–306, doi:10.1063/1.555632.

[7] Putintsev NM, Putintsev DN. High-frequency dielectric permittivity of water and its components. *Russ. J. Phys. Chem.* 2011;85:1113–8, doi:10.1134/S0036024411070272.

[8] SMA Solar Technology AG. *Technical Information - Leading Leakage Currents*. Available at: https://files.sma.de/dl/7418/Ableitstrom-TI-en-26.pdf [accessed 28.08.2020].

[9] HASEGAWA Y, Ohki Y, FUKUNAGA K, MIZUNO M, SASAKI K. Complex Permittivity Spectra of Various Insulating Polymers at Ultrawide-Band Frequencies. *Electr Eng Jpn* 2017;198:11–8, doi:10.1002/eej.22925.

[10] Wang J, Shi K. Study of polymer humidity sensor array on silicon wafer. *Journal of Materials Science* 2004:3155–7.

[11] Boudaden J, Steinmaßl M, Endres H-E, Drost A, Eisele I, Kutter C, Müller-Buschbaum P. Polyimide-Based Capacitive Humidity Sensor. *Sensors (Basel)* 2018;18.